# research papers

# Structural basis for the autoinhibition of the C-terminal kinase domain of human RSK1

**Dan Li,[a]‡§ Tian-Min Fu,[a]‡
Jie Nan,[a] Cong Liu,[a]§ Lan-Fen Li[a]
and Xiao-Dong Su[a,b]***

[a]State Key Laboratory of Protein and Plant Gene Research, School of Life Sciences, Peking University, Beijing 100871, People's Republic of China, and [b]Peking University Shenzhen Graduate School, Shenzhen 518055, People's Republic of China

‡ These authors contributed equally to this work.
§ Current address: UCLA–DOE Institute for Genomics and Proteomics, University of California, Los Angeles, Los Angeles, California, USA.

Correspondence e-mail: xdsu@pku.edu.cn

p90 ribosomal S6 kinases (RSKs) respond to various mitogen stimuli and comprise two distinct protein kinase domains. The C-terminal kinase domain (CTKD) receives signal from ERK1/2 and adopts an autoinhibitory mechanism. Here, the crystal structure of human RSK1 CTKD is reported at 2.7 Å resolution. The structure shows a standard kinase fold, with the catalytic residues in the ATP-binding cleft orientated in optimal conformations for phosphotransfer. The inactivation of the CTKD is conferred by an extra $\alpha$-helix ($\alpha$L), which occupies the substrate-binding groove. In combination with previous knowledge, this structure indicates that activation of RSK1 involves the removal of $\alpha$L from the substrate-binding groove induced by ERK1/2 phosphorylation.

## 1. Introduction

The p90 ribosomal S6 kinases (RSKs), which are downstream effectors of the mitogen-activated protein kinase signalling pathway, comprise a family of Ser/Thr kinases that are involved in the regulation of various cellular processes such as cell growth, cell proliferation and cell survival (Roux & Blenis, 2004; Anjum & Blenis, 2008). In humans, this family contains four isoforms (RSK1–4) and two structurally related cousins known as mitogen and stress-activated kinases 1 and 2 (MSK1 and MSK2; Anjum & Blenis, 2008; Deak *et al.*, 1998; New *et al.*, 1999). The four isoforms of human RSK are highly similar in sequence and domain organization. Human RSKs comprise two non-identical kinase domains linked by a conserved loop of about 100 amino acids (Jones *et al.*, 1988; Fisher & Blenis, 1996). The N-terminal kinase domain of RSK (NTKD) belongs to the AGC kinase family and is responsible for the phosphorylation of substrates. The C-terminal kinase domain of RSK (CTKD) shares homology with kinases of the calcium/calmodulin-dependent family (Jones *et al.*, 1988) and is involved in autophosphorylation. The activation of RSK starts with the docking of extracellular signal-regulated kinase 1/2 (ERK1/2) onto the RSK C-terminal tail to activate RSK CTKD. The activated RSK CTKD self-phosphorylates the linker region between the NTKD and the CTKD. The phosphorylated linker region is able to recruit 3'-phospho-inositide-dependent kinase 1 (PDK1), which subsequently phosphorylates RSK NTKD. As a result, RSK is fully activated to phosphorylate its downstream substrates such as oestrogen receptor $\alpha$, cyclic AMP response element-binding protein, c-Fos and the mitotic checkpoint kinase to modulate

diverse cellular processes (Bjørbaek *et al.*, 1995; Xing *et al.*, 1996; De Cesare *et al.*, 1998; Schwab *et al.*, 2001; Joel *et al.*, 1998).

As a member of the RSK family, RSK1 plays an important role in many cellular processes. RSK1 is expressed ubiquitously in almost all human tissues, predominantly in kidney, lung and pancreas (Zeniou *et al.*, 2002). Recent studies have shown that RSK1 is overexpressed in primary breast and prostate cancers and is a possible anticancer target (Clark *et al.*, 2005). Crystal structures of inactivated human RSK1 NTKD bound to various ligands have been determined (Ikuta *et al.*, 2007). Here, we present the crystal structure of human RSK1 CTKD at 2.7 Å resolution. The structure shows autoinhibition of RSK1 CTKD by its $\alpha$L helix, suggesting that ERK1/2 may activate RSK1 by phosphorylating RSK1 followed by the displacement of $\alpha$L from its inhibitory position. A similar regulatory mechanism has been observed previously in MAP KAP kinase 2 (MK2; Meng *et al.*, 2002) and murine RSK2 CTKD (Malakhova *et al.*, 2008). The atomic structure of human RSK1 CTKD is of great interest in order to understand the mechanism of RSK activation and for structure-based anticancer-drug development.

## 2. Materials and methods

### 2.1. Protein preparation, crystallization and data collection

Protein preparation, crystallization and data collection have been reported previously (Fu *et al.*, 2007). In brief, human RSK1 CTKD (RSK1 411–735) was overexpressed in *Escherichia coli* Rosetta strain at 291 K. The protein was purified by nickel-chelating chromatography followed by gel filtration. The purified protein was concentrated to 5 mg ml$^{-1}$ in buffer consisting of 20 m$M$ sodium citrate pH 6.0 for crystallization. Crystals were obtained in 20 m$M$ HEPES pH 7.5, 17%($w/v$) PEG 3350, 4%($v/v$) acetonitrile by the sitting-drop vapour-diffusion method at 290 K. Crystals were directly flash-cooled in liquid nitrogen before data collection. Diffraction data were collected at 100 K on beamline 3W1A at the Beijing Synchrotron Radiation Facility (BSRF) and processed using *HKL*-2000 (Otwinowski & Minor, 1997). Data-collection statistics are given in Table 1.

### 2.2. Structure determination

Initial phases were obtained by molecular replacement with *MOLREP* (Vagin & Teplyakov, 2010) using the structure of murine RSK2 CTKD (PDB entry 2qr7; Malakhova *et al.*, 2008) as the search model. The sequence identity between human RSK1 CTKD and murine RSK2 CTKD is 81%. Model building was performed with *Coot* (Emsley & Cowtan, 2004) and was illustrated with *PyMOL* (DeLano, 2002). Crystallographic refinement was performed with *phenix.refine* (Adams *et al.*, 2002) and *BUSTER-TNT* (Bricogne *et al.*, 2009). The model was finally refined to an $R_{\text{work}}$ of 18.8% and an $R_{\text{free}}$ of 23.8% to 2.7 Å resolution. Coordinates have been deposited with PDB code 3rny. Statistics of structure refinement are given in Table 1.

**Table 1**
X-ray data-collection and refinement statistics.

Values in parentheses are for the highest resolution shell.

| | |
|---|---|
| Crystal parameters | |
|   Space group | $P2_1$ |
|   Unit-cell parameters (Å, °) | $a = 39.86$, $b = 143.47$, $c = 59.92$, $\alpha = \gamma = 90.0$, $\beta = 95.8$ |
|   Molecules in asymmetric unit | 2 |
| Data collection | |
|   Synchrotron beamline | 3W1A, BSRF |
|   Wavelength (Å) | 0.98 |
|   Resolution (Å) | 50–2.7 (2.80–2.70) |
|   Reflections (observed/unique) | 48516/17784 |
|   Completeness (%) | 97.9 (97.6) |
|   $R_{\text{merge}}$† (%) | 7.8 (34.8) |
|   $\langle I/\sigma(I)\rangle$ | 9.8 (3.5) |
| Refinement | |
|   Resolution (Å) | 2.7 |
|   $R_{\text{work}}$‡ (%) | 18.8 |
|   $R_{\text{free}}$§ (%) | 23.8 |
|   No. of non-H atoms | |
|     Protein | 4025 |
|     Ions | 2 Na$^+$ |
|     Waters | 43 |
|   $B$ factors (Å$^2$) | |
|     Protein | 46.6 |
|     Waters | 24.6 |
|   R.m.s. deviations | |
|     Bond lengths (Å) | 0.010 |
|     Bond angles (°) | 1.210 |
|   Ramachandran plot¶ (%) | |
|     Preferred regions | 95.53 |
|     Allowed regions | 3.50 |
|     Outliers | 0.97 |

† $R_{\text{merge}} = \sum_{hkl}\sum_i |I_i(hkl) - \langle I(hkl)\rangle|/\sum_{hkl}\sum_i I_i(hkl)$. ‡ $R_{\text{work}} = \sum_{hkl} ||F_{\text{obs}}| - |F_{\text{calc}}||/\sum_{hkl} |F_{\text{obs}}|$. § $R_{\text{free}} = \sum_{hkl} ||F_{\text{obs}}| - |F_{\text{calc}}||/\sum_{hkl} |F_{\text{obs}}|$ calculated using a random set containing 5% of the reflections that were not included throughout structure refinement. ¶ Calculated using *PROCHECK* (Laskowski *et al.*, 1993).

## 3. Results and discussion

### 3.1. Overall structure of RSK1 CTKD

The structure of human RSK1 CTKD is a typical bilobed kinase fold consisting of a smaller N-terminal lobe (N lobe) and a larger C-terminal lobe (C lobe) (Fig. 1*a*). The N lobe is composed of a five-stranded antiparallel $\beta$-sheet ($\beta$1–$\beta$5) and one prominent $\alpha$-helix ($\alpha$C). The C lobe, which is responsible for substrate recognition, is predominantly composed of $\alpha$-helices. There are two molecules (chains *A* and *B*) in the asymmetric unit. The disulfide bond between the Cys579 residues observed in the RSK2 CTKD crystallographic dimer (corresponding to Cys575 in RSK1 CTKD) was not clearly observed in the structure of RSK1 CTKD. In solution, the gel-filtration elution profile showed a major peak corresponding to monomeric RSK1 CTKD, indicating that the protein functions as a monomer (Supplementary Fig. S1[1]). Chains *A* and *B* in the asymmetric unit are essentially identical, with an r.m.s.d. (root-mean-square deviation) of 0.07 Å for 259 aligned C$^\alpha$ atoms; therefore, only chain *B* was used for analysis of the RSK1 CTKD structure in this paper. Some loop regions, including part of the 'activation loop', are missing in our

[1] Supplementary material has been deposited in the IUCr electronic archive (Reference: XB5047). Services for accessing this material are described at the back of the journal.
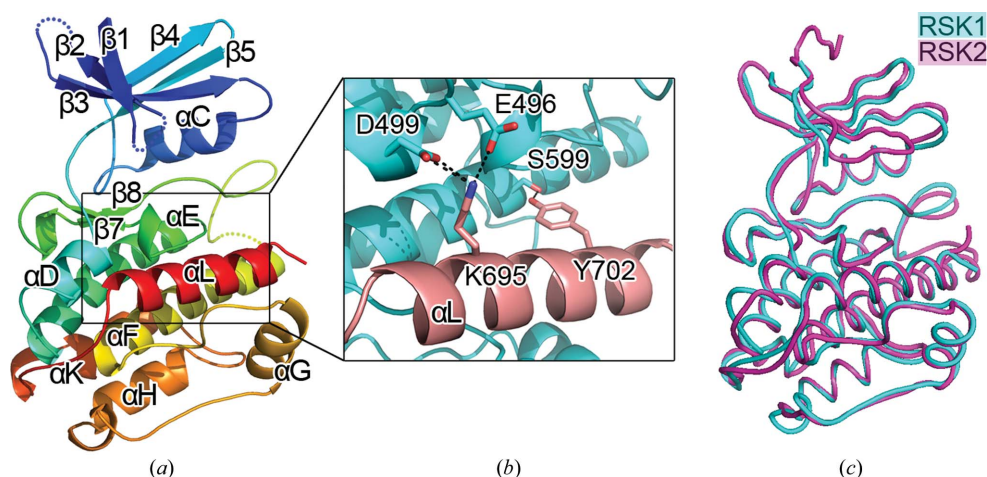
**Figure 1**
(a) Overall structure of human RSK1 CTKD. Missing regions are indicated by dotted lines. (b) The interactions of the inhibitory αL helix (pink) with the rest of the structure (cyan). (c) Superimposition of the CTKDs of RSK1 (cyan) and RSK2 (magenta; PDB entry 2qr7).
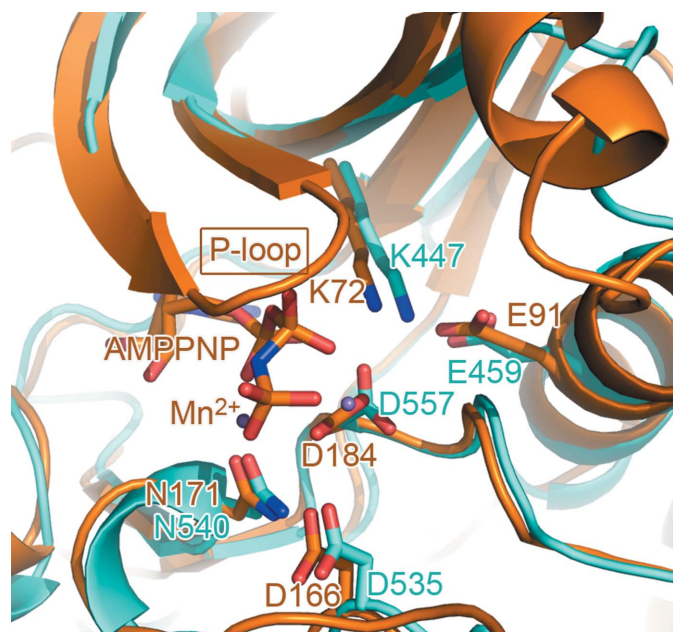


**Figure 2**
Superimposition of the ATP-binding clefts of RSK1 CTKD (cyan) and PKA (orange; PDB entry 1cdk; Bossemeyer *et al.*, 1993). The P loop in RSK1 CTKD is disordered. The catalytic residues which are required for optimal phosphotransfer are shown as sticks and labelled.

structure owing to poor electron density (Supplementary Table S1). An extra C-terminal α-helix (αL) embedded in a cradle formed by the αF–αG junction is a distinct structural feature that may confer the regulatory property of RSK1.

### 3.2. ATP-binding cleft

The ATP-binding cleft is located between the two lobes. The highly conserved phosphate-binding loop (P loop) between $\beta1$ and $\beta2$ is highly flexible in the absence of ATP (Huse & Kuriyan, 2002). In our RSK1 CTKD structure the glycine-rich motif in the P loop (residues 425–431) is dis-

ordered (Figs. 1a and 2). A precise spatial arrangement of the catalytic residues is required for optimal phosphotransfer (Huse & Kuriyan, 2002). In the structure of RSK1 CTKD the residues Asp535 in the RD motif, Asp557 in the DFG motif, Lys447 in the $\beta3$ strand and Glu459 in the αC helix, which are essential for catalysis in the ATP-binding cleft, share similar conformations with those in active cyclic AMP-dependent protein kinase (PKA; Fig. 2). Therefore, the ATP-binding cleft of RSK1 CTKD is structured ready for phosphotransfer catalysis.

### 3.3. Glu496 is not essential for autoinhibition of human RSK1

Sequence alignment shows that the CTKDs of RSKs share a high degree of sequence identity (Fig. 3), indicating similar three-dimensional structures. The sequence identity between human RSK1 CTKD and murine RSK2 CTKD is 81%. Therefore, it is not surprising that the overall structure of human RSK1 CTKD closely resembles that of murine RSK2 CTKD (Fig. 1c). Overlay of the two structures results in an r.m.s.d. of 0.7 Å for backbone $C^{\alpha}$ atoms. Differences between the two structures mainly lie in loop regions (Fig. 1c).

*In vitro* and *in vivo* studies have shown that the truncation or mutation of a putative autoinhibitory α-helix results in constitutive activation of RSK2 CTKD (Poteet-Smith *et al.*, 1999). The crystal structure of murine RSK2 CTKD revealed that the inhibitory α-helix (αL) occupies a 'cradle' shaped by the αF–αG junction. Compared with PKA, αL shifts αD away from the catalytic cleft and results in the reorientation of Glu500 (Malakhova *et al.*, 2008). Lys700 captures Glu500, forming an ionic pair and inhibiting Glu500 from binding to ATP, revealing the structural basis of RSK2 autoinhibition (Malakhova *et al.*, 2008; Fig. 4a). In contrast, despite the high structural similarity between RSK1 and RSK2 CTKDs, Glu496 of RSK1 is still in the ATP-binding position, as is the analogous Glu127 of active PKA. The difference in glutamate orientation between RSK1 and RSK2 is mainly caused by the mutation of Pro696 in RSK2 to Leu691 in RSK1 (Figs. 4b

and 4c). Pro696 and Arg507 of RSK2 form a stable packing interaction (Misura *et al.*, 2004) and attract Asp503 to form an ionic interaction. Thus, Glu500 has sufficient space to interact with Lys700.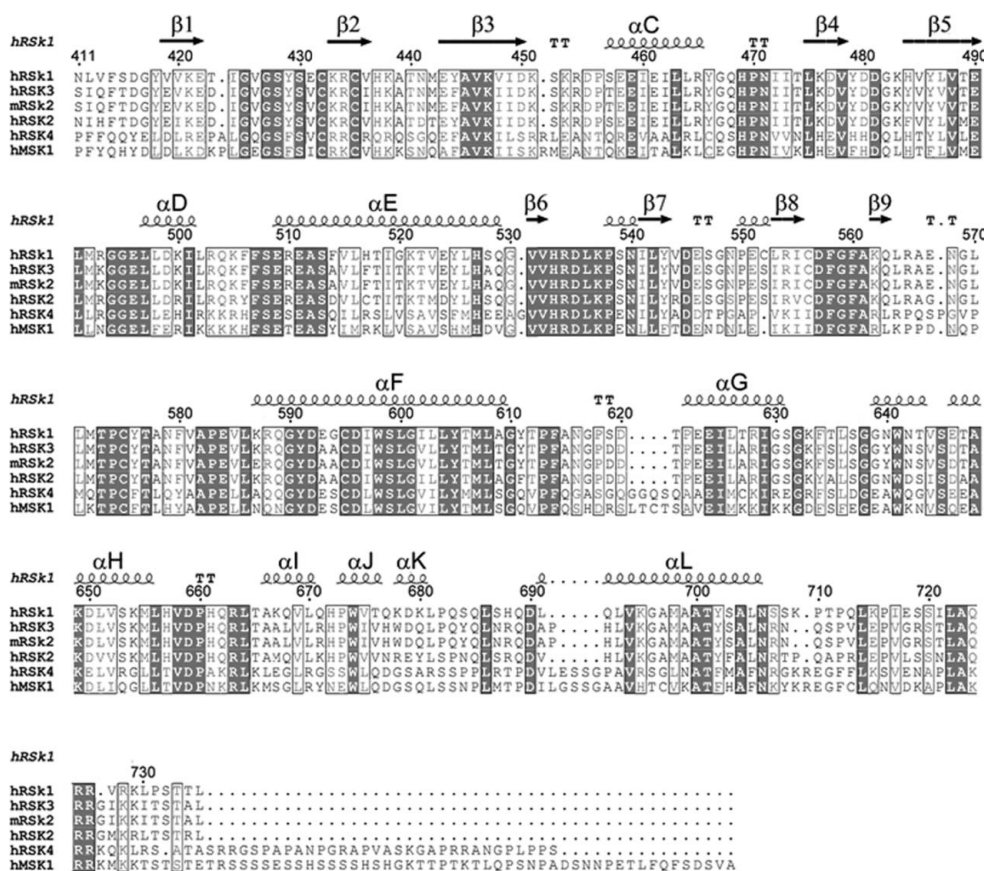 In RSK1, Leu691 takes the place of Pro696 in RSK2. The hydrophobic leucine side chain extrudes between Asp499 and Arg503 and breaks the ionic interaction. Instead, Asp499 is rearranged to interact with Lys695. The ionic interaction between Glu496, Asp499 and Lys695 constrains Glu496 in the favourable ATP-binding conformation.

Therefore, unlike in the case of murine RSK2, the autoinhibition of αL in human RSK1 is not defined by Glu496.

### 3.4. αL occupies the substrate-binding groove

Several Ser/Thr kinases have been reported to adopt a negative regulatory mechanism, including PKA (Zheng *et al.*, 1993; Bossemeyer *et al.*, 1993), Ca$^{2+}$/calmodulin-dependent protein kinase (CaMKI; Goldberg *et al.*, 1996), titin (Mayans *et al.*, 1998) and MAP KAP kinase 2 (MK2; Meng *et al.*, 2002; Underwood *et al.*, 2003). MK2 is closely related to RSK1 CTKD in structure and in regulatory mechanism. Their sequence identity is 34.4%. Overlay of the two structures



**Figure 3**
Sequence alignment of the C-terminal kinase domains of human RSK1–4 (hRSK1–4), human MSK1 (hMSK1) and murine RSK2 (mRSK2).
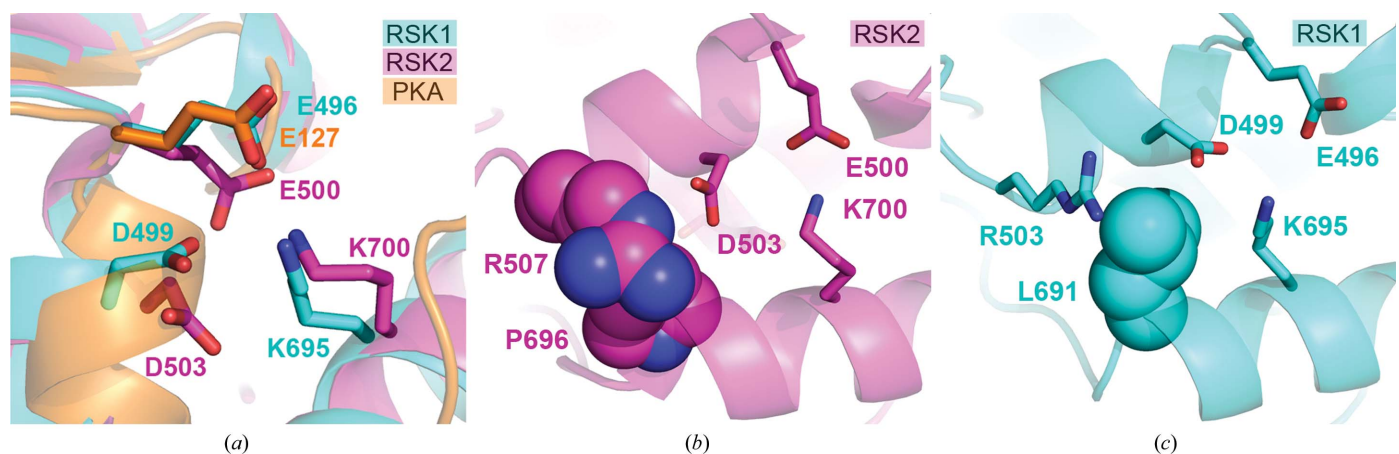


**Figure 4**
Orientation and interaction of Glu496. (*a*) Comparison of Glu496 in RSK1 (cyan) with analogous residues in RSK2 (magenta) and active PKA (orange; PDB entry 1cdk). Glu496 of RSK1 is in the ATP-binding position, as is the analogous Glu127 of active PKA. In contrast, the analogous Glu500 of RSK2 is orientated away from the ATP-binding position and forms an ionic interaction with Lys700. The different orientation of the glutamate in RSK1 and RSK2 is mainly caused by the mutation of Pro696 in RSK2 to Leu691 in RSK1. (*b*) Pro696 and Arg507 of RSK2 (spheres) form a stable packing and attract Asp503, forming an ionic interaction. Thus, Glu500 has space to interact with Lys700. The same view of RSK1 is shown in (*c*) and shows that Leu691 (spheres) breaks the interaction between Asp499 and Arg503 and forces Asp499 to interact with Lys695. The ionic interaction between Glu496, Asp499 and Lys695 constrains Glu496 in the ATP-binding conformation.

resulted in an r.m.s.d. of 1.146 Å over 216 $C^\alpha$ atoms. In addition, the structural phases of RSK1 CTKD can also be obtained by using the coordinates of MK2 (PDB entry 1kwp; Meng *et al.*, 2002) as the search model for molecular replacement. The C-terminal regulatory domain of MK2 (residues 328–400) forms α-helical structures and occupies the substrate-binding groove, acting as a pseudo-substrate (Meng *et al.*, 2002; Fig. 5). Deletion of this domain resulted in activation of the catalytic activity (Zu *et al.*, 1995). Similarly, truncation of αL in RSK2 resulted in constitutive activation of the CTKD (Poteet-Smith *et al.*, 1999). In our crystal structure of RSK1 CTKD αL is linked by a loop to the rest of the domain and sits in the putative substrate-binding groove, forming nearly the same conformation as αK in MK2 (Fig. 5) and indicating that RSK1 and MK2 share a similar autoinhibitory mechanism. The inhibitory αL in RSK1 CTKD is fixed and orientated by ionic interactions between Glu496, Asp499 and Lys695 and by hydrogen bonding between Ser599 and Tyr702 (Fig. 1*b*). Mutation of Tyr707 in RSK2 (equivalent to Tyr702 in RSK1) to Ala resulted in activation of the CTKD (Poteet-Smith *et al.*, 1999). The structure of PKA complexed
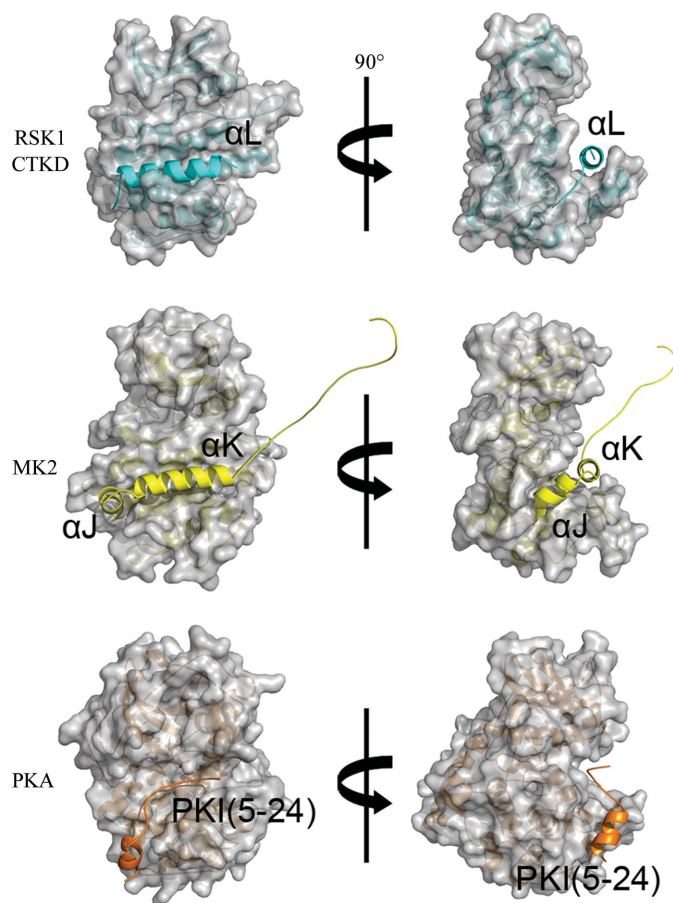
with peptide consensus sequence PKI(5–24) revealed an extended conformation of the substrate analogue along the binding groove (Bossemeyer *et al.*, 1993), whereas in RSK1 CTKD the binding groove was blocked by αL, suggesting that the autoinhibition of RSK1 is mainly caused by inhibition of peptide substrate binding (Fig. 5). Biochemical and structural studies have shown synergistic effects of peptide and MgATP binding (Bossemeyer *et al.*, 1993). Therefore, owing to the inhibition of substrate binding by αL, ATP binding is less favoured. We attempted to obtain the structure of RSK1 CTKD in complex with ATP or ATP analogues by soaking and cocrystallization, but failed. The same problem was experienced with murine RSK2 (Malakhova *et al.*, 2008).

RSK activation requires ordered phosphorylation mediated by ERK1/2 and phosphoinositide-dependent protein kinase 1 (PDK1) and RSK autophosphorylation (Cargnello & Roux, 2011). *In vivo* studies have shown that RSK and ERK1/2 form an inactive complex in quiescent cells (Hsiao *et al.*, 1994; Zhao *et al.*, 1996), suggesting that binding of ERK1/2 cannot replace the inhibitory αL in RSK activation. The activation of RSKs requires the phosphorylation of Thr573 in the activation loop of CTKD and of Thr359/Ser363 in the linker region by ERK1/2 upon mitogenic stimulation (Cargnello & Roux, 2011; Ranganathan *et al.*, 2006; Smith *et al.*, 1999; Sutherland *et al.*, 1993; Dalby *et al.*, 1998). Therefore, rather than displacing αL from the substrate-binding groove of RSK, ERK1/2 initiates RSK activation by phosphorylation. The phosphorylated RSK may undergo a dramatic conformational change and remove αL from the substrate-binding groove. Alternatively, the phosphorylated sites may increase the substrate-binding affinity and thus the binding of the native substrate to αL.

**Figure 5**
Surface representation of the substrate-binding groove. The inhibitory α-helices in RSK1 (αL, cyan) and MK2 (αJ and αK, yellow; PDB entry 1kwp) occupy the substrate-binding grooves, resulting in inactivation of the kinases. The pseudo-substrate PKI(5–24) fits in the substrate-binding groove of PKA (orange; PDB entry 1cdk), resembling the binding of the native substrate sequence.

### References

Adams, P. D., Grosse-Kunstleve, R. W., Hung, L.-W., Ioerger, T. R., McCoy, A. J., Moriarty, N. W., Read, R. J., Sacchettini, J. C., Sauter, N. K. & Terwilliger, T. C. (2002). *Acta Cryst.* D**58**, 1948–1954.
Anjum, R. & Blenis, J. (2008). *Nature Rev. Mol. Cell Biol.* **9**, 747–758.
Bjørbaek, C., Zhao, Y. & Moller, D. E. (1995). *J. Biol. Chem.* **270**, 18848–18852.
Bossemeyer, D., Engh, R. A., Kinzel, V., Ponstingl, H. & Huber, R. (1993). *EMBO J.* **12**, 849–859.
Bricogne, G., Blanc, E., Brandl, M., Flensburg, C., Keller, P., Paciorek, W., Roversi, P., Sharff, A., Smart, O. S., Vonrhein, C. & Womack, T. O. (2009). *BUSTER-TNT.* Cambridge: Global Phasing Ltd.
Cargnello, M. & Roux, P. P. (2011). *Microbiol. Mol. Biol. Rev.* **75**, 50–83.

Clark, D. E., Errington, T. M., Smith, J. A., Frierson, H. F., Weber, M. J. & Lannigan, D. A. (2005). *Cancer Res.* **65**, 3108–3116.

Dalby, K. N., Morrice, N., Caudwell, F. B., Avruch, J. & Cohen, P. (1998). *J. Biol. Chem.* **273**, 1496–1505.

Deak, M., Clifton, A. D., Lucocq, L. M. & Alessi, D. R. (1998). *EMBO J.* **17**, 4426–4441.

De Cesare, D., Jacquot, S., Hanauer, A. & Sassone-Corsi, P. (1998). *Proc. Natl Acad. Sci. USA*, **95**, 12202–12207.

DeLano, W. L. (2002). *PyMOL.* http://www.pymol.org.

Emsley, P. & Cowtan, K. (2004). *Acta Cryst.* D**60**, 2126–2132.

Fisher, T. L. & Blenis, J. (1996). *Mol. Cell. Biol.* **16**, 1212–1219.

Fu, T.-M., Li, D., Nan, J., Li, L., Xue, Y. & Su, X.-D. (2007). *Acta Cryst.* F**63**, 1026–1028.

Goldberg, J., Nairn, A. C. & Kuriyan, J. (1996). *Cell*, **84**, 875–887.

Hsiao, K.-M., Chou, S.-Y., Shih, S.-J. & Ferrell, J. E. Jr (1994). *Proc. Natl Acad. Sci. USA*, **91**, 5480–5484.

Huse, M. & Kuriyan, J. (2002). *Cell*, **109**, 275–282.

Ikuta, M., Kornienko, M., Byrne, N., Reid, J. C., Mizuarai, S., Kotani, H. & Munshi, S. K. (2007). *Protein Sci.* **16**, 2626–2635.

Joel, P. B., Traish, A. M. & Lannigan, D. A. (1998). *J. Biol. Chem.* **273**, 13317–13323.

Jones, S. W., Erikson, E., Blenis, J., Maller, J. L. & Erikson, R. L. (1988). *Proc. Natl Acad. Sci. USA*, **85**, 3377–3381.

Laskowski, R. A., MacArthur, M. W., Moss, D. S. & Thornton, J. M. (1993). *J. Appl. Cryst.* **26**, 283–291.

Malakhova, M., Tereshko, V., Lee, S.-Y., Yao, K., Cho, Y.-Y., Bode, A. & Dong, Z. (2008). *Nature Struct. Mol. Biol.* **15**, 112–113.

Mayans, O., van der Ven, P. F., Wilm, M., Mues, A., Young, P., Fürst, D. O., Wilmanns, M. & Gautel, M. (1998). *Nature (London)*, **395**, 863–869.

Meng, W., Swenson, L. L., Fitzgibbon, M. J., Hayakawa, K., Ter Haar, E., Behrens, A. E., Fulghum, J. R. & Lippke, J. A. (2002). *J. Biol. Chem.* **277**, 37401–37405.

Misura, K. M., Morozov, A. V. & Baker, D. (2004). *J. Mol. Biol.* **342**, 651–664.

New, L., Zhao, M., Li, Y., Bassett, W. W., Feng, Y., Ludwig, S., Padova, F. D., Gram, H. & Han, J. (1999). *J. Biol. Chem.* **274**, 1026–1032.

Otwinowski, Z. & Minor, W. (1997). *Methods Enzymol.* **276**, 307–326.

Poteet-Smith, C. E., Smith, J. A., Lannigan, D. A., Freed, T. A. & Sturgill, T. W. (1999). *J. Biol. Chem.* **274**, 22135–22138.

Ranganathan, A., Pearson, G. W., Chrestensen, C. A., Sturgill, T. W. & Cobb, M. H. (2006). *Arch. Biochem. Biophys.* **449**, 8–16.

Roux, P. P. & Blenis, J. (2004). *Microbiol. Mol. Biol. Rev.* **68**, 320–344.

Schwab, M. S., Roberts, B. T., Gross, S. D., Tunquist, B. J., Taieb, F. E., Lewellyn, A. L. & Maller, J. L. (2001). *Curr. Biol.* **11**, 141–150.

Smith, J. A., Poteet-Smith, C. E., Malarkey, K. & Sturgill, T. W. (1999). *J. Biol. Chem.* **274**, 2893–2898.

Sutherland, C., Campbell, D. G. & Cohen, P. (1993). *Eur. J. Biochem.* **212**, 581–588.

Underwood, K. W. *et al.* (2003). *Structure*, **11**, 627–636.

Vagin, A. & Teplyakov, A. (2010). *Acta Cryst.* D**66**, 22–25.

Xing, J., Ginty, D. D. & Greenberg, M. E. (1996). *Science*, **273**, 959–963.

Zeniou, M., Ding, T., Trivier, E. & Hanauer, A. (2002). *Hum. Mol. Genet.* **11**, 2929–2940.

Zhao, Y., Bjorbaek, C. & Moller, D. E. (1996). *J. Biol. Chem.* **271**, 29773–29779.

Zheng, J., Knighton, D. R., ten Eyck, L. F., Karlsson, R., Xuong, N., Taylor, S. S. & Sowadski, J. M. (1993). *Biochemistry*, **32**, 2154–2161.

Zu, Y.-L., Ai, Y. & Huang, C.-K. (1995). *J. Biol. Chem.* **270**, 202–206.